 https://doi.org/10.3311/PPee.21420

Periodica Polytechnica Electrical Engineering and Computer Science, 68(1), pp. 54–63, 2024

Analysis and Design of Voltage-controller Based on Single-state Feedback Active Damping for Grid-forming Converters

Fateh Abdoune[1*], Issam Abadlia[1], Antar Beddar[1], Linda Hassaine[1], Mohamed Reda Bengourina[1]

[1] Centre de Développement des Énergies Renouvelables, 16032 Bouzaréah, Algiers, P.O.B. 62, Algeria
[*] Corresponding author, e-mail: f.abdoune@cder.dz

Received: 29 October 2022, Accepted: 07 July 2023, Published online: 28 August 2023

Abstract

This paper investigates the analysis and design of digital single-loop voltage-controller for grid-forming voltage source converters with *LC*-filters. Inspired by the structure diagram of the passive damping method, the virtual resistance concept based on only capacitor voltage feedback is used to realize active damping without the need of any current sensor, reducing thus the system costs. It is revealed from the controller closed-loop analysis that the insertion of an integrator in series with a proportional and resonant controller can significantly improve stability margin and dynamic performance of the system, then only the proportional controller need to be determined for system stability and the resonant controller is merely used for zero steady-state tracking error, which facilitates the controller parameter tuning. A systematic design based on the root contours in the discrete z-domain is proposed to optimize the parameters of the controller. The largest distance between the poles of the closed-loop system and the unit circle is achieved, which indicates the fastest dynamic performance under desired stability margins. Meanwhile, a simple differentiator constructed by backward-Euler plus lead-compensator is used to replace the noise-sensitive derivative term. In order to evaluate the proposed control approach performance, the system is tested in laboratory setup under different load conditions. The obtained results verify the effectiveness of the proposed design method and validate the analysis.

Keywords

grid-forming voltage source converters, active damping, voltage controller, stability design, fast dynamic response

1 Introduction

The renewable energy sources, such as wind power and photovoltaic power, are generally connected to the grid by voltage source converters (VSCs). They are generally working as current sources, i.e., grid-following converters. However, for some cases, such as in weak grids or islanded distributed generator systems, supporting the grid voltage is required, and thus the voltage-controlled VSCs, which is also known as grid-forming converters (GFCs), are increasingly deployed and emerge as a new trend [1–4]. To provide a pure voltage output with small switching harmonics, LC-type output filters are commonly employed as well as the filter capacitor voltage is controlled to supply uninterrupted power to the local loads. However, the filter inherent resonance brings a stability challenge to the control system [4–7] and consequently, how to design satisfactory control systems achieving adequate stability margins, fast dynamic responses, and negligible steady-state errors becomes a critical challenge for these VSCs.

Many linear control methods have been reported in the literature to meet the requirements of GFCs. They are categorized into two groups in respect to the control structure, i.e., the single and dual-loop control schemes. The single-loop control schemes have been investigated due to the simple control design and free of current sensors for active damping [8–12]. It is revealed that proportional and resonant (PR) controller can stabilize the control system when LC-filter resonant frequency is above one-third of the sampling frequency, which is usually too high to get satisfied switching harmonic attenuation performance in practice. To further widen the stability design region of LC-filters, several strategies have been proposed. In [10], a PR controller with a negative proportional gain is employed at the expense of a poor dynamic response of the controller. Besides, a damping controller based on lead filters [11] or low-pass feed-forward of the capacitor voltage [12] was developed to actively damp the

Cite this article as: Abdoune, F., Abadlia, I., Beddar, A., Hassaine, L., Bengourina, M. R. "Analysis and Design of Voltage-Controller Based on Single-state Feedback Active Damping for Grid-forming Converters", Periodica Polytechnica Electrical Engineering and Computer Science, 68(1), pp. 54–63, 2024. https://doi.org/10.3311/PPee.21420

inherent resonance without the need of current feedback. Nevertheless, more control parameters are introduced by these methods, which make system design substantially complicated. The dual-loop control schemes are more popularly employed [13–20], which consist of an outer capacitor voltage-loop and an inner inductor or capacitor current-loop. It has been proved that the inclusion of the inner current-loop can provide the necessary damping and facilitate the over-current protection of the VSCs [19]. However, having an inner-loop current controller requires more sensors that increases the overall cost and reduces the system reliability. Optimized parameter design of the dual-loop control structure has always been an attractive topic for researchers [13–20]. There are no widely accepted guidelines to design control parameters to ensure the system stability. Most of the existing design approaches focus more on the voltage outer-loop where PR controller is usually employed. Generally, the voltage outer-loop is designed to achieve a specified bandwidth and disturbance rejection requirements whereas the inner current control loop is only considered to support and facilitate the design of the outer loop to get a desired performance [15]. Nevertheless, due to the inter-coupling between the two loops, this result in a complex design process where is difficult to analyze how each control parameter affects the stability of the VSC system [16, 20]. Therefore, only both optimized control loops can result in an optimal control system performance.

In this work, unlike the classical nested-loop approach mentioned above, the control objective is achieved by considering both the voltage loop and the virtual resistor (VR) based active damping (AD) controller as a single controller with only the capacitor voltage feedback, this can be saving system cost by eliminating the need of current sensor. Firstly, according to the analysis of the basic damping solutions, the AD scheme with only capacitor voltage feedback is selected. The digital implementation of this scheme needs to find a physically realizable term to replace noise-sensitive derivative term in AD controller. Then, the closed-loop controller analysis is presented, and intrinsic time delay of the controller is investigated, from which an extra integrator in series with a basic PR controller is proposed for improving the system stability and dynamic performance. A systematic design approach based on the root contours in discrete z-domain is proposed to optimize the parameters of the resulted controller. The largest distance between the poles of the closed-loop system and the unit circle is achieved, which indicates the strongest damping and fastest dynamic response. Finally, in order to evaluate the proposed control approach performance, a single-phase VSC system is tested under inductive, capacitive and nonlinear load conditions. Experimental results are provided to verify the theoretical findings and the effectiveness of the proposed design approach.

2 System description and modeling

Fig. 1 shows the typical topology of three-phase VSC currently utilized in islanded microgrids. It consists of a DC power source, a three-phase two-level inverter, a second order *LC*-filter and local loads, which can be linear or nonlinear. For this investigation, it is assumed that the input dc bus voltage can be supplied constant by a renewable energy source or battery energy storage system, and the parasitic resistors of the filter components are neglected to emulate a worst resonance case of the system.

In this paper, PR controllers in the stationary frame will be studied, since it can be easily implemented in both single and multi-phase systems. Based on Fig. 1, three equivalent per-phase circuits can be obtained. For the sake of simplicity, all the analysis will be performed here for only one phase. The plant model required to design the proposed voltage controller relates the controller output voltage with the capacitor voltage. Using the notation and current flow indicated in the Fig. 1 and taking Laplace transformation, the output voltage dynamics of the GFC is given as:

$$v_c(s) = G_{vc}(s) \times v_i(s) - G_{vi}(s) \times i_l(s), \tag{1}$$

where $G_{vc}(s)$ and $G_{vi}(s)$ are the transfer functions from converter-side voltage to capacitor voltage and from load current to capacitor voltage respectively, expressed as:

$$G_{vc}(s) = \frac{v_c(s)}{v_i(s)} = \frac{\omega_r^2}{s^2 + \omega_r^2}, \tag{2}$$

$$G_{vi}(s) = \frac{v_c(s)}{i_l(s)} = \frac{sL_f\omega_r^2}{s^2 + \omega_r^2}, \tag{3}$$

and $\omega_r = \sqrt{1/L_f C_f}$ is the resonance frequency of the *LC*-filter.

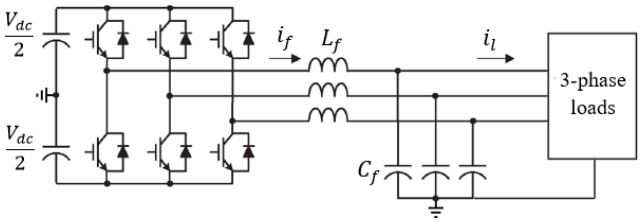

Fig. 1 Topology of three-phase VSC system with output *LC*-filter

Such a model depends on the current demanded by the unknown load connected across the VSC. This current is modelled as an independent disturbance input, which enables passive or active loads or external grid connection to be considered. As illustrated by system Bode diagram presented in Fig. 2, significant changes in the plant dynamics, especially the effective resonant frequency of the system, are caused when different types of linear loads are connected. It can be seen that for no-load condition, $G_{vc}(s)$ has always one pair of conjugate poles, leading to system instability. Resistive loads would provide physical damping to the control system, contributing thus to system stability. However, pure inductive and capacitive loads shift the resonant frequency of the system; this deteriorates the robust performance of the controller severely as well as overall system stability [10]. It is thus necessary to provide the voltage controller with enough robust performance under a wide range of loads to deal with system uncertainty caused by load variation.

3 Proposed control approach

An approach for developing the forms of AD controller is investigated in Section 3, where the main idea is to relate the control diagram with the expected equivalent circuit by manipulating the block diagrams without changing the transient behavior of the system. Two main criteria, which are the transient behavior of power stage and the number of measuring sensors, are considered to select a preferred AD controller.

3.1 Developing of AD controller

According to the physical location of the resistor in the *LC* circuit, there are four basic damping solutions, i.e., resistor either in series or in parallel with the filter inductor or capacitor. Based on the frequency responses of these four connections shown in Fig. 3, it can be seen that resistor in series with *C* or in parallel with *L* will weaken the high-frequency harmonic attenuating ability of *LC*-filter, which results in a relatively low voltage control bandwidth. On the contrary, when resistor is added in parallel with *C* either in series with *L*, it is clear that these connections only have a positive effect while keeping unchanged the magnitude-frequency characteristics of *LC*-filter at the low- and high-frequency ranges, which is convenient for the design of the voltage controller. As a result, the two last connections are preferred among the possible connection types.

The implementation of a VR that is connected in series to the *L* requires an additional current sensor. Considering that the inductor current is already measured for protection purpose in dual-loop control scheme, so this is the better option. On the contrary, the implementation of a VR that is connected in parallel with *C* does not need an additional sensor; because the voltage sensor is already exists and an extra sensor can be saved. However, a differentiator is required to convert the current signal to the voltage signal that can be applied to the pulse width modulation (PWM), which may bring a noise amplification problem in practical implementation [21, 22]. One way to overcome it is to feed back the capacitor current, instead of voltage, which presently, has many damping methods based on it [16, 19], but will nonetheless incur additional sensor cost.

Based on the above analysis, the AD scheme with only the capacitor voltage feedback to realize VR in parallel with the filter-capacitor can be regarded as the preferred choice when simultaneously taking into account the two predefined criteria. The corresponding per-phase block diagram for the proposed control is shown in Fig. 4, in which the capacitor voltage is fed-back for both output voltage regulation and AD purposes.

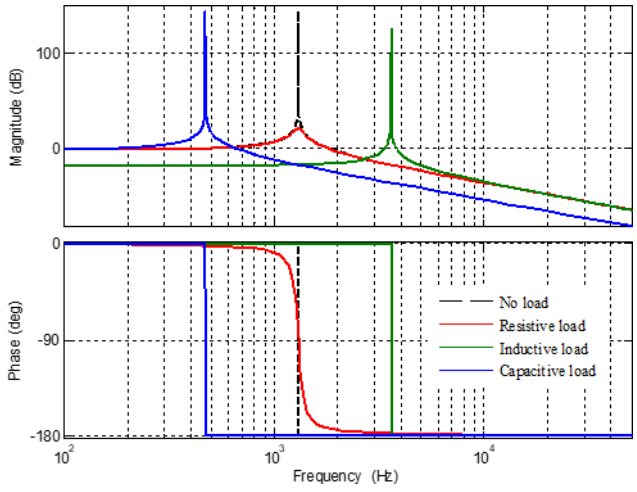

Fig. 2 Bode of the plant model under different type of loads

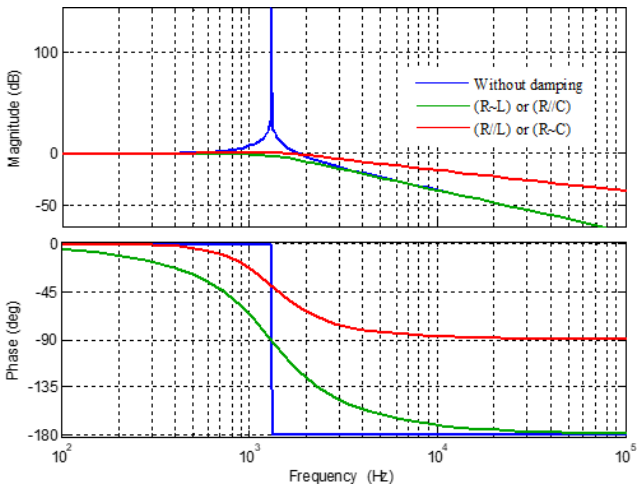

Fig. 3 Impact of resistor location in damping the transient oscillations

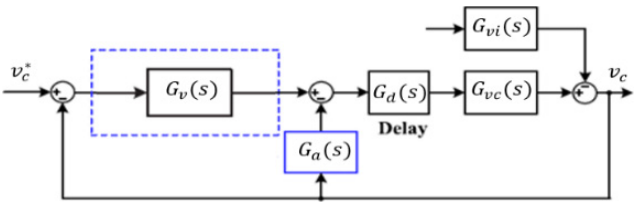

Fig. 4 Block diagram of the proposed control scheme in s-domain

In Fig. 4, $G_d(s)$ represents the control loop delay which is the 1.5 sampling periods delay consisting of one sampling period of computation delay and equivalent half sampling period of zero-order-hold (ZOH) effect in PWM delays [23]. In the continuous s-domain analysis, the time delay effect is always approximated by the rational transfer functions, where the second order Padé approximation is widely used [18]. $G_v(s)$ is the capacitor voltage controller, which is generally implemented with a PR controller to achieve accurate AC voltage reference tracking. As shown in Fig. 4, an AD controller is equipped with the voltage feedback loop to realize VR in parallel with filter capacitor without the need of current feedback. From the block transformation, the AD function can be expressed as:

$$G_a(s) = k_d \times C_f \times s. \tag{4}$$

Considering first that the AD feedback function as an ideal differentiation of the capacitor voltage, it can be easily identified that the proposed control scheme is equivalent to a traditional dual-loop control scheme with capacitor current feedback, where the damping gain k_d can be regarded as the proportion gain of the inner loop controller. Thus, the same closed loop transfer function and so the same control effects can be achieved. It should be noticed that in practice such similarities can be obtained by only an accurate derivative approximation term, which will be addressed later in Section 3.2. From the Fig. 4, the open-loop transfer function with AD controller in Laplace frequency domain can be derived as:

$$T_{ov}(s) = G_v(s) \times \frac{G_d(s)G_{vc}(s)}{1 + G_a(s)G_d(s)G_{vc}(s)}. \tag{5}$$

Frequency domain synthesis techniques can now be applied to the voltage control loop. However, the computation delay and PWM modulation would introduce a transcendental function to the open-loop transfer function, which makes it hard to analyze the stability of the control system [10, 14]. To solve this problem, the control block diagram in Fig. 4 can be transformed from s-domain into z-domain. The discretized form of the open-loop transfer function can be derived by applying ZOH transformation:

$$T_{ov}(z) = G_v(z) \times \frac{z^{-1}G_{vc}(z)}{1 + z^{-1}G_a(z)G_{vc}(z)}. \tag{6}$$

Since the control scheme will finally be implemented in a digital processor, the stability of the overall control system can be assessed by this last equation.

3.2 Analysis of the closed-loop controller

Considering the effect of time delay, it has been found that the proposed voltage-loop control as that the traditional dual-loop control is unstable when the *LC*-filter resonance frequency is higher than one-sixth of the sampling frequency [5, 10]. To ensure a stable control loop, this paper considers first that the *LC*-filter is designed with a resonance frequency less than one-sixth of the sampling frequency. The parameters used in the analysis and calculation in this article are listed in Table 1.

For the entire voltage-loop system given by Eq. (5), it is seen from the denominator that the damping gain can dampen the LC resonant peak and the voltage loop can hence be designed with satisfactory stability margin, e.g., widely accepted criteria: PM > 30° and GM > 3dB [16]. The larger gain k_d is, the more damping will be added. However, considering the system time delay there is additional phase-lag present in the voltage loop, which limits the design of the damping gain. As can be seen from the frequency responses of the uncompensated voltage-loop plotted in Fig. 5, there exists an upper limit for k_d to avoid the non-minimum phase (NMP) behavior, which is not desired in the control system. Below this value, the *LC* resonance is slightly shifted yet still significant, and around the resonant frequency the phase will cross over $-\pi$, which may lead to a relatively low control loop bandwidth when basic PR is used as the voltage controller.

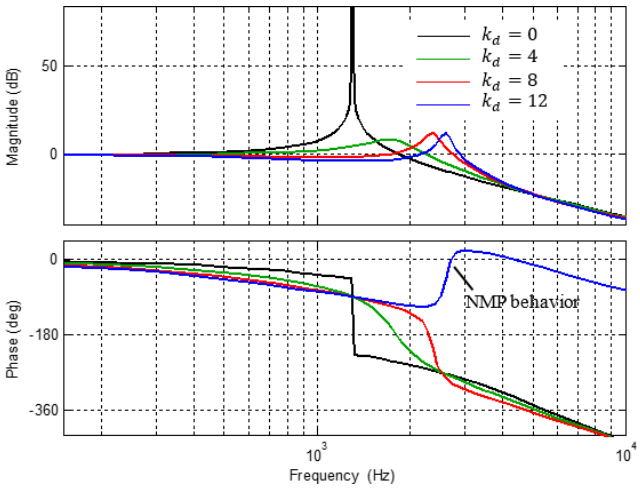

Fig. 5 Frequency responses of the uncompensated voltage-loop with different damping gains

It is found in some published papers that higher values of proportional gain of PR controller increase the T_{ov} high-frequencies gains, which reduces the phase margin and results in unstable closed-loop response. Hence, to guarantee the system stability, the designed proportional gain is generally very small, which means that its enlarging effectiveness the control bandwidth is very limited [13, 16]. It is identified that the phase lag of the R controller plays a critical role in stabilizing the system. In contrast, adding the P controller can only reduce the phase lag of the R controller and worst the system stability. This demerit can be overcome by modifying the voltage controller structure. It is proposed in this paper that an extra integrator is inserted in series with the basic PR controller. The objective is to guarantee a decreasing frequency response, enhance the system control bandwidth, as well as for fast load steps disturbances rejection. As a result, a PRI controller is obtained, whose transfer function can be expressed as:

$$G_v(s)=\left(k_p+\frac{k_r s}{s^2+2\zeta\omega_1 s+\omega_1^2}\right)\times\left(\frac{1}{s}\right), \tag{7}$$

where k_p and k_r are respectively the proportional and resonant gains of the basis PR controller, ω_1 is the fundamental frequency and ζ is the damping ratio of the resonant compensator, whose value is set 0.01 to preserve certain adaptability toward frequency variations.

The analysis above elaborates that the basic PR voltage controller limits the control bandwidth of the voltage loop. To illustrate this drawback, the frequency responses of the compensated open-loop system with respectively the R, PR and PRI controllers are plotted together in Fig. 6. The used controllers' parameters are given in Table 1, where those the PR controller are chosen only as an indication to make a comparison and show his drawbacks on the system stability. It is obvious that due to the introduced integral behavior, the R and PRI controllers are capable of effectively damp the resonance without comprising the system bandwidth. As it can be seen, the attainable maximum bandwidth with these controllers is much larger than that the PR one, then the requirement of stability margins can be easily satisfied. It is worth noting that for frequencies above ω_1, the R and PRI controllers can be approximated as integral ones. This equivalence indicates that both the controllers with the same parameters achieve similar performance even though the low frequency behavior of each controller is substantially different. Consequently, only the k_p gain in Eq. (7) should be designed for system stability, whose value is not affected by ω_1 as in case that using only R controller. The k_r gain can merely be designed for zero steady-state error, yet with little phase effect at the phase crossover frequency. When necessary, additional resonant terms can be included for removing distortion harmonics introduced by the non-linear loads without affecting system stability margin [22].

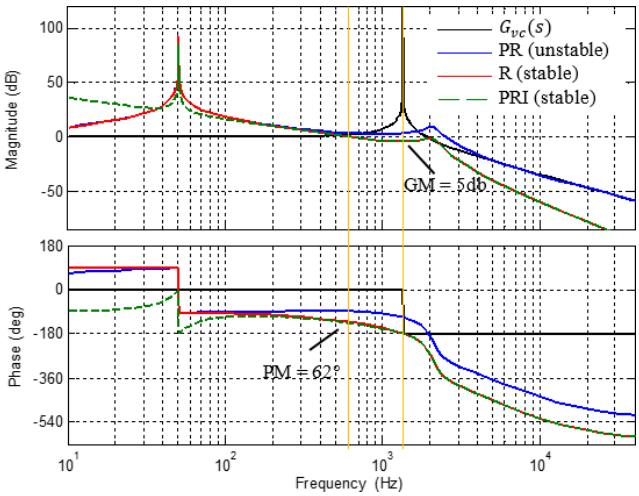

Fig. 6 Frequency responses of the compensated voltage loop with respectively R, PR and PRI controllers

3.3 Implementation of digital differentiator

As mentioned above, there exists a pure differentiator in the AD controller, which cannot be directly implemented due to unacceptable noise amplification. Thus, the first practical issue of the proposed control scheme is the implementation of this digital differentiator. Among the existing direct methods, it is known that Backward Euler derivative is the only stable derivative, but it introduces a phase lag up to 90° at the Nyquist frequency, which is equivalent to a delay of half sampling period [21]. This phase-lag will eventually nullify the derivative effect, implying lack of accuracy. An intuitive idea to match the ideal differentiator closely is to compensate this half sampling period. To do that, a lead-lag element, a first-order lead compensator and a second order generalized integrator are used [24, 25]. Due to its effectiveness and simplicity, the first-order lead compensator is preferred here. A direct realization of digital differentiator based on backward Euler plus first order lead compensator is constructed as:

$$G_s(z)=z\left(\frac{1+m}{z+m}\right)\times\left(\frac{z-1}{zT_s}\right);\ 0\le m\le 1. \tag{8}$$

The proposed differentiator can be regarded as a general form of digital differentiator, whose performance can be flexibly adjusted depending on the value of m. Obviously, for m closer to 0, it is reduced to backward Euler differentiator and for m closer to 1 it behaves more like Tustin

differentiator. Therefore, a trade-off between the phase lead compensation and the gain amplification should be made to select a proper m. The value $m = 0.8$ is selected here as it gives a closer match with the ideal differentiator.

4 Controller parameters design

Assuming that the output filter components have already been determined, only the two controller gains k_d and k_p can change the closed-loop poles and thus the dynamic performance and stability. A systematic design approach for these two parameters is formulated below based on the root contours in the discrete z-domain. The fastest dynamic response under desired stability margins is defined as the criteria in order to determine the optimized performance. Therefore, a pole map of uncompensated voltage loop can be directly employed to get the optimized k_d that results in dominating poles nearest to the original point of the unit circle. In this manner, the design of the damping loop is completely independent from that of the voltage loop.

Fig. 7 illustrates the pole map of the uncompensated voltage loop obtained by varying the gain k_d from 0 to 15. It can be observed that a pair of resonant poles moves toward to the inside of the unit circle at the beginning, which is theoretically beneficial for the design of voltage controller. In fact, the moving inside the unit circle is the contribution of the active damping. However, with increasing k_d continuously, the damped poles move toward the unit circle and come out the unit circle at a certain extent. Once these poles stay out of the unit circle, the NMP system behaviour results, which is not preferred since it leads to the voltage loop hard to be stable. It should be noted that when $k_d = 7$, the dominant poles are closest to the original point, which means that the VSC can obtain best damping effect and can result in the fastest dynamic performance for the damping loop. To better identify this optimized gain, the damping rate is calculated according to the closed-loop poles using a simple program in MATLAB.

In the same way, since the resonance term in Eq. (7) only affects the frequency response near the frequency ω_1, hence, only the parameter k_p needs to tune in the outer voltage loop for satisfying the desired stability margins. First, the influence of the resonance term is neglected, that is to consider the voltage controller as integral one, which is discretized by the Tustin method, as shown in Eq. (9):

$$G_v(s) \simeq \frac{k_p}{s};\ s \leftarrow \frac{2}{T_s}\frac{z-1}{z+1}. \tag{9}$$

On the other hand, the damping loop controller takes the optimized gain k_{do} previously determined. As a result, the optimized gain k_{po} can be easily obtained with the help of pole map of $T_{ov}(z)$ plotted in Fig. 8 with varying the gain k_p from 0 to 600. It can be observed that with the increase of k_p, a pair of dominant poles initially moves towards original point, and then these poles move gradually away and come out the unit circle when k_p increases to a certain extend. When $k_p = 300$, the poles are closest to the original point of the unity circle. If this value can ensure satisfied stability margins as illustrated in Fig. 6 (GM = 5 dB and PM = 62° at 600 Hz), it is deemed as the optimized one because of the fastest voltage loop dynamic performance.

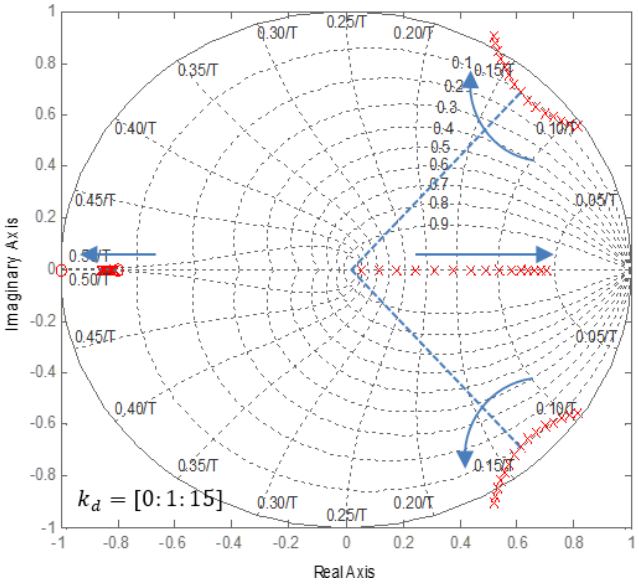

Fig. 7 Pole map of the uncompensated voltage-loop varying with k_d

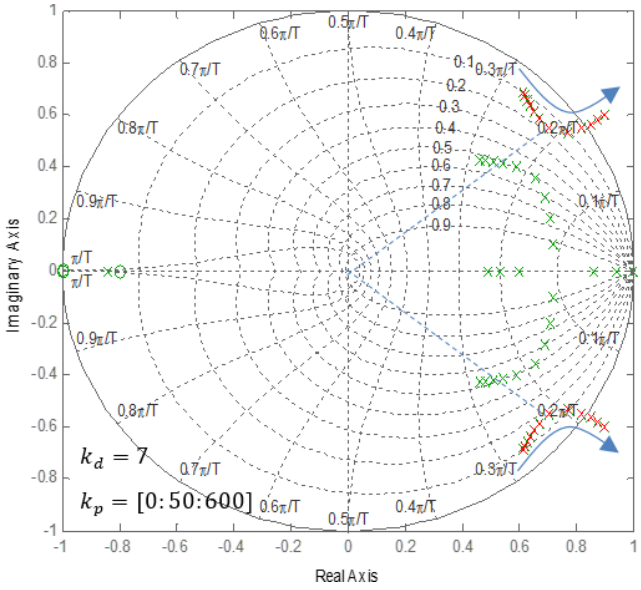

Fig. 8 Pole map of the compensated voltage-loop varying with k_p

5 Experimental verification and results

Effectiveness of the proposed controller design has been verified experimentally on the laboratory prototype with a single-phase *LC* filtered inverter setup. The parameters of the experimental setup are listed in Table 1. The proposed closed-loop control is implemented with dSPACE DS1202 platform whose output gating signals are channeled to SEMIKRON inverter. A constant DC voltage power supply was used to power the VSC. A 4-channels oscilloscope and a power quality analyzer were employed to capture and analysis the experimental waveforms.

Table 1 System and control parameters of the experimental setup

Parameters	Value
AC peak output voltage	100 V
AC fundamental frequency	50 Hz
Inverter DC-link voltage	110 V
LC output filter inductance	1 mH
LC output filter capacitance	15 µF
Sampling and switching frequency	10 kHz
Inductive load (series RL)	$R = 25\ \Omega$; $L = 6$ mH
Capacitive load (parallel RC)	$R = 20\ \Omega$; $C = 50$ µF
Nonlinear load (diode bridge with *LC*)	$L = 6$ mH; $C = 50$ µF; $R = 20\ \Omega$
Optimized damping gain	$k_d = 7$
PR controller gains	$k_p = 0.9$; $k_r = 300$
PRI controller gains	$k_p = 300$; $k_r = 900$

5.1 Performance of GFC turns on and off without load

Under the above designed parameters, the first test shows the reference voltage tracking capability with the proposed control, where the system is operated with a sinusoidal reference voltage under the no-load condition. This is one critical situation in practical applications because of the lowest system damping. Fig. 9 shows the experimental transient waveforms obtained when turns on and off the GFC with changing the damping gain from 4 to 7 and 10, respectively. In order to assess the dynamic performance, the voltage tracking error (Δv) is displayed together with the output voltage in each case. The settling time is utilized to qualify the dynamic speed of the control system. It is defined as the time from the step change to the final value within an error band less than 5% of the steady state value.

As can be seen, the system dynamic response becomes slow with the increase or decrease of the damping gain from its optimized value. The settling time is above 5 ms for a low damping gain ($k_d = 4$). In addition, apparent high frequency oscillations appear in output voltage during both GFC activation and deactivation events, which indicating that the system is marginally stable. For a large damping gain ($k_d = 10$), there is visible voltage tracking error (voltage total harmonic distortion (THD = 4.9%), which indicate that AD is not efficient. With the optimized damping gain ($k_d = 7$), the system dynamic response is very

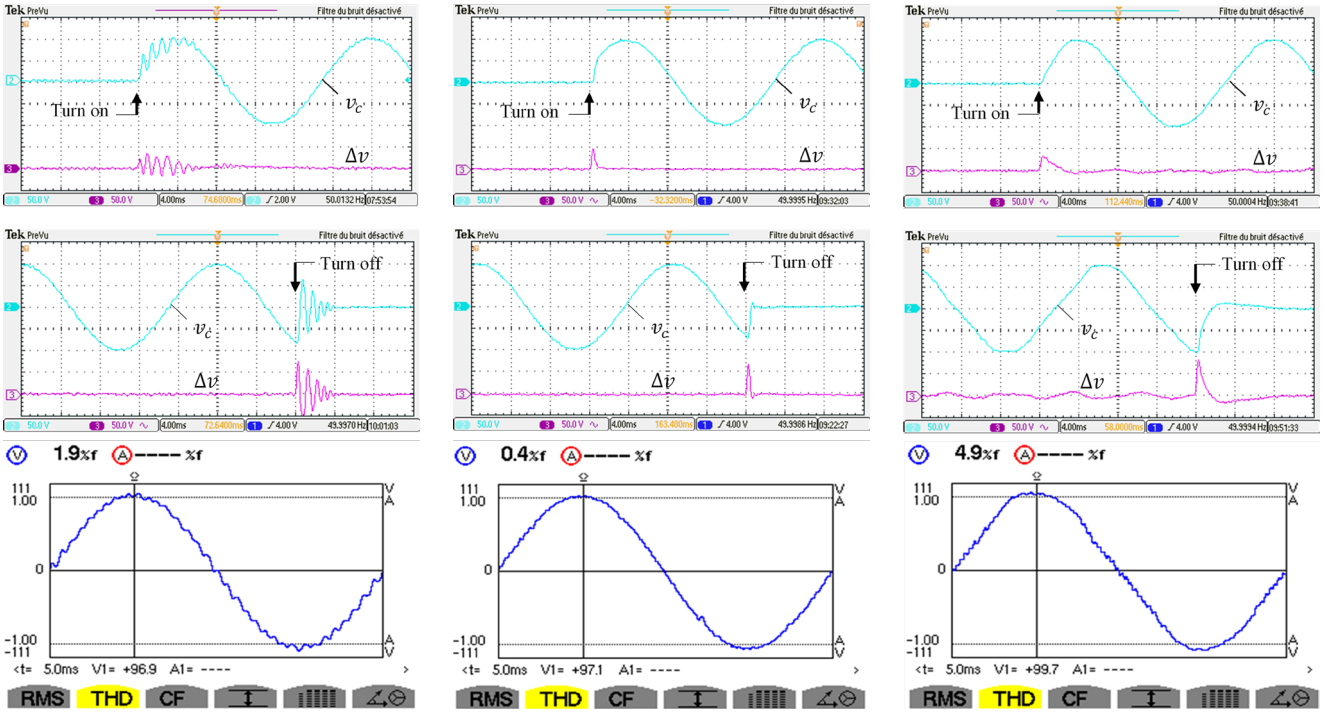

Fig. 9 Transient performance of VSC turns on and off without load for different damping gains: Ch2 denotes v_c and Ch3 denotes Δv (50 V/div); (a) case $k_d = 4$, (b) case $k_d = 7$, (c) case $k_d = 10$

fast, and the settling time is only about 1 ms. Moreover, the control system is capable of providing a high-waveform quality voltage. This statement is verified by the low output voltage THD (0.40%).

5.2 Performance of GFC with load turns on and off

The second test evaluates the performance of the proposed controller under inductive, capacitive and nonlinear load steps. The parameter details of the tested loads are given in Table 1. Both the connection and the disconnection events are tested when the GFC is operated for nominal reference voltage. Fig. 10 shows transient experimental waveforms of the output voltage and the load current when the loads are suddenly turned on and off respectively. As can be seen from Fig. 10, no significant transients are observed in the output voltage during both the loads connection and disconnection events and the system responds quickly against the load disturbances, which verify the robustness of the system. It should be noted that the experimental results in Fig. 10 are obtained without incorporating any additional resonant terms to the controller. From the voltage and current steady state THD analysis, a very low distortion in voltage output is observed even with high distorting load consisting of a diode rectifier bridge feeding *LC*-filter in parallel with resistor at DC-link. This is due to the high gain at lower frequencies inherent to the high bandwidth controller design. In regard to the paralleled RC load (capacitive load), the capacitor of the load would share switching current harmonics with the capacitor of the *LC*-filter. As can be seen in Fig. 10(b), the total load current also contains large amounts of switching harmonics. Additionally, the loads are connected to the VSC through a manual switch, and due to the jitter of the manual switch during switching on, the large load current spikes appear in this case of capacitive load.

6 Conclusion

This article demonstrates the design and implementation of digital single-loop voltage controller for grid-forming VSCs. Although the proposed control scheme does not require current measurement, which reduces the system costs and enhances the reliability, a wide bandwidth and cost-effective sensor should be used in order to incorporate over-current protection. The discrete model of the plant is firstly developed, and then the tuning of the controller parameters is discussed based on the discrete root locus analysis to achieve the fastest dynamic performance under desired stability margins. The proposed design process is very simple without solving complex formulas and the tuning of the inner damping loop is completely independent from that of the voltage outer loop. The experimental results provided show a good dynamic response and proves the effectiveness of the designed controller. The obtained results with linear and non-linear loads validate the ability to provide the high quality of output voltage even in the presence of low order harmonics in the load current.

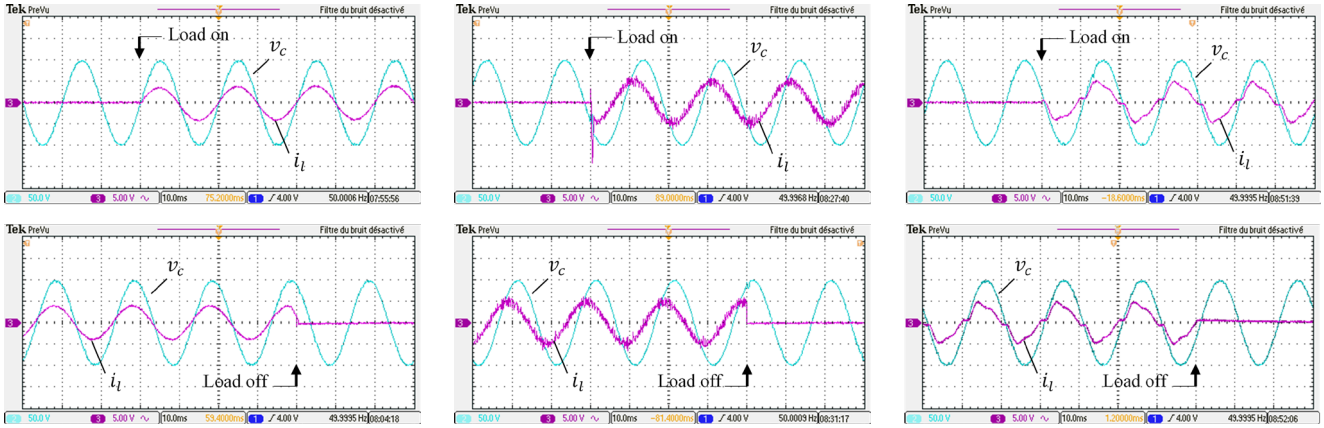

(a) (b) (c)

Fig. 10 Transient performance of VSC under inductive, capacitive and nonlinear load steps: v_c (50 V/div), i_l (5 A/div), time (10 ms/div); (a) Inductive load steps; (b) Capacitive load steps; (c) Nonlinear load steps

References

[1] Rocabert, J., Luna, A., Blaabjerg, F., Rodríguez, P. "Control of power converters in AC microgrids", IEEE Transactions on Power Electronics, 27(11), pp. 4734–4749, 2012. https://doi.org/10.1109/TPEL.2012.2199334

[2] Pérez-Estévez, D., Doval-Gandoy, J., Guerrero, J. M. "AC-voltage harmonic control for stand-alone and weak-grid-tied converter", IEEE Transactions on Industry Applications, 56(1), pp. 403–421, 2019. https://doi.org/10.1109/TIA.2019.2942265

[3] Zhang, H., Xiang, W., Lin, W., Wen, J. "Grid forming converters in renewable energy sources dominated power grid: Control strategy, stability, application, and challenges", Journal of Modern Power Systems and Clean Energy, 9(6), pp. 1239–1256, 2021. https://doi.org/10.35833/MPCE.2021.000257

[4] Rosso, R., Wang, X., Liserre, M., Lu, X., Engelken, S. "Grid-forming converters: An overview of control approaches and future trends", In: 2020 IEEE Energy Conversion Congress and Exposition (ECCE), Detroit, MI, USA, 2020, pp. 4292–4299. ISBN 978-1-7281-5827-3 https://doi.org/10.1109/ECCE44975.2020.9236211

[5] Zhou, Z., Li, X., Lu, X., Liu, Y., Shen, G., Wu, X. "Stability blind-area-free control design for microgrid-interfaced voltage source inverters under dual-mode operation", IEEE Transactions on Power Electronics, 35(11), pp. 12555–12569, 2020. https://doi.org/10.1109/TPEL.2020.2988565

[6] Li, Y. W. "Control and resonance damping of voltage-source and current-source converters with *LC* filters", IEEE Transactions on Industrial Electronics, 56(5), pp. 1511–1521, 2009. https://doi.org/10.1109/TIE.2008.2009562

[7] Dahono, P. A., Bahar, Y. R., Sato, Y., Kataoka, T. "Damping of transient oscillations on the output LC filter of PWM inverters by using a virtual resistor", In: 4th IEEE International Conference on Power Electronics and Drive Systems. IEEE PEDS 2001 - Indonesia. Proceedings (Cat. No.01TH8594), Denpasar, Indonesia, 2001, pp. 403–407. ISBN 0-7803-7233-6 https://doi.org/10.1109/PEDS.2001.975347

[8] Li, Z., Li, Y., Wang, P., Zhu, H., Liu, C., Gao, F. "Single-loop digital control of high-power 400-Hz ground power unit for airplanes", IEEE Transactions on Industrial Electronics, 57(2), pp. 532–543, 2010. https://doi.org/10.1109/TIE.2009.2033490

[9] Liu, T., Wang, X. "Transient stability of single-loop voltage-magnitude controlled grid-forming converters", IEEE Transactions on Power Electronics, 36(6), pp. 6158–6162, 2021. https://doi.org/10.1109/TPEL.2020.3034288

[10] Li, X., Lin, P., Tang, Y., Wang, K. "Stability design of single-loop voltage control with enhanced dynamic for voltage-source converters with a low LC-resonant-frequency", IEEE Transactions on Power Electronics, 33(11), pp. 9937–9951, 2018. https://doi.org/10.1109/TPEL.2018.2794066

[11] de Souza, I. D. N., de Almeida, P. M., Barbosa, P. G., Duque, C. A., Ribeiro, P. F. "Digital single voltage loop control of a VSI with LC output filter", Sustainable Energy, Grids and Networks, 16, pp. 145–155, 2018. https://doi.org/10.1016/j.segan.2018.07.004

[12] Wang, X., Loh, P. C., Blaabjerg, F. "Stability analysis and controller synthesis for single-loop voltage-controlled VSIs", IEEE Transactions on Power Electronics, 32(9), pp. 7394–7404, 2017. https://doi.org/10.1109/TPEL.2016.2632065

[13] Deng, H., Fang, J., Qi, Y., Tang, Y., Debusschere, V. "A generic voltage control for grid-forming converters with improved power loop dynamics", IEEE Transactions on Industrial Electronics, 70(4), pp. 3933-3943, 2023. https://doi.org/10.1109/TIE.2022.3176308

[14] Monfared, M., Golestan, S., Guerrero, J. M. "Analysis, design, and experimental verification of a synchronous reference frame voltage control for single-phase inverters", IEEE Transactions on Industrial Electronics, 61(1), pp. 258–269, 2014. https://doi.org/10.1109/TIE.2013.2238878

[15] Zhao, Z., Chi, J. "Analysis and tuning of dual-loop control for grid-forming converters in the discrete-time domain", In: 2021 IEEE 12th Energy Conversion Congress & Exposition - Asia (ECCE-Asia), Singapore, Singapore, 2021, pp. 2268–2273. ISBN 978-1-7281-6345-1 https://doi.org/10.1109/ECCE-Asia49820.2021.9479346

[16] Wang, J., Chen, L., Liu, Z., Zhang, Z., Zhang, X. "Optimized Parameter Design of the Dual-Loop Control for Grid-Forming VSCs With *LC* Filters", IEEE Transactions on Industry Applications, 58(1), pp. 820–829, 2022. https://doi.org/10.1109/TIA.2021.3121345

[17] Geng, Y., Yun, Y., Chen, R., Wang, K., Bai, H., Wu, X. "Parameters design and optimization for LC-type off-grid inverters with inductor-current feedback active damping", IEEE Transactions on Power Electronics, 33(1), pp. 703–715, 2018. https://doi.org/10.1109/TPEL.2017.2664812

[18] Siraj, H., McGrath, B. P., Nutkani, I. U., Liao, Y., Wang, X. "Analytical control system synthesis for dual-loop cascaded stationary frame voltage regulators", In: 2020 IEEE Energy Conversion Congress and Exposition (ECCE), Detroit, MI, USA, 2020, pp. 2598–2605. ISBN 978-1-7281-5827-3 https://doi.org/10.1109/ECCE44975.2020.9236392

[19] Erdocia, J., Urtasun, A., Marroyo, L. "Dual voltage–current control to provide grid-forming inverters with current limiting capability", IEEE Journal of Emerging and Selected Topics in Power Electronics, 10(4), pp. 3950–3962, 2022. https://doi.org/10.1109/JESTPE.2021.3133806

[20] Han, Y., Jiang, A.-T., Coelho, E. A. A., Guerrero, J. M. "Optimal performance design guideline of hybrid reference frame based dual-loop control strategy for stand-alone single-phase inverters", IEEE Transactions on Energy Conversion, 33(2), pp. 730–740, 2018. https://doi.org/10.1109/TEC.2017.2769114

[21] Xin, Z., Wang, X., Loh, P. C., Blaabjerg, F. "Realization of digital differentiator using generalized integrator for power converters", IEEE Transactions on Power Electronics, 30(12), pp. 6520–6523, 2015. https://doi.org/10.1109/TPEL.2015.2442414

[22] Abdoune, K., Abdoune, F., Aouzellag, D., Ghedamsi, K. "Improved Voltage Harmonics Compensation Strategy for a Stand-Alone DFIG Operating under Unbalanced and Nonlinear Load Conditions", Periodica Polytechnica Electrical Engineering and Computer Science, 64(2), pp. 144–156, 2020.
https://doi.org/10.3311/PPee.15029

[23] de Bosio, F., de Souza Ribeiro, L. A., Freijedo, F. D., Pastorelli, M., Guerrero, J. M. "Effect of state feedback coupling and system delays on the transient performance of stand-alone VSI with LC output filter", IEEE Transactions on Industrial Electronics, 63(8), pp. 4909–4918, 2016.
https://doi.org/10.1109/TIE.2016.2549990

[24] Xin, Z., Loh, P. C., Wang, X., Blaabjerg, F., Tang, Y. "Highly accurate derivatives for LCL-filtered grid converter with capacitor voltage active damping", IEEE Transactions on Power Electronics, 31(5), pp. 3612–3625, 2016.
https://doi.org/10.1109/TPEL.2015.2467313

[25] Pan, D., Ruan, X., Wang, X. "Direct realization of digital differentiators in discrete domain for active damping of *LCL*-type grid-connected inverter", IEEE Transactions on Power Electronics, 33(10), pp. 8461–8473, 2018.
https://doi.org/10.1109/TPEL.2017.2780174